# Effective static and high-frequency viscosities of concentrated suspensions of soft particles

Carlos I. Mendoza[a)]
*Department of Physics and Astronomy, University of Pennsylvania, Philadelphia, PA 19104, USA and Instituto de Investigaciones en Materiales, Universidad Nacional Autónoma de México, Apdo. Postal 70-360, 04510 México, D.F., Mexico*

(Received 27 March 2011; accepted 19 July 2011; published online 5 August 2011)

We obtain an analytic expression that allows to determine the static $\eta$ and high-frequency $\eta_\infty$ viscosities as function of the volume fraction $\phi$ of a concentrated suspension of soft spherical particles in a liquid of viscosity $\eta_0$. The particles consist of a hard core of radius $a$ covered by a porous layer of thickness $d$. Suspensions of hard spheres and homogeneous porous particles are limiting cases of the model. The proposed expression incorporates the results for the intrinsic viscosity obtained on the basis of a cell model [H. Ohshima, Langmuir **26**, 6287 (2010)] into a recently obtained relation for the effective viscosity of concentrated colloidal suspensions [C. I. Mendoza and I. Santamaría-Holek, J. Chem. Phys. **130**, 044904 (2009); J. Colloid. Interface Sci. **346**, 118 (2010)]. In this model, the correlations between the particles due to crowding effects are introduced through an effective volume fraction $\phi_{eff}$ which is then used as integration variable in a differential effective medium procedure. The final expression is simple, accurate, and allows to collapse all the data in a universal master curve that is independent of the parameters characterizing the system. The only difference between the static and high-frequency cases is that in the later case $\phi_{eff}$ also incorporates hydrodynamic interactions arising from the so-called relaxation term. We have tested the accuracy of our model comparing with experimental results for spherical polymeric brushes and simulations for the high-frequency viscosity of homogeneous porous particles. In all cases the agreement with the data is extremely good. © *2011 American Institute of Physics*. [doi:10.1063/1.3623472]

## I. INTRODUCTION

The ability to tune the viscosity of suspensions of colloidal particles plays a major role in many technological applications, where the precise control of the flow properties is essential. When particles are suspended in an homogeneous isotropic fluid, the viscosity of the resulting suspension is larger than the viscosity of the original liquid. In the case of dilute suspensions of hard spherical particles, the viscosity $\eta(\phi)$ as a function of the volume fraction $\phi$ of the particles was first derived by Einstein[1] and is given by the expression

$$\eta(\phi) = \eta_0 \left(1 + \frac{5}{2}\phi\right), \tag{1}$$

where $\eta_0$ is the viscosity of the original fluid. Various extensions of Eq. (1) to calculate the viscosity of dilute suspensions of particles other than rigid spheres have been proposed. Among them we can mention the case of solid ellipsoidal particles,[2] emulsions of spherical droplets,[3] homogeneously porous rigid spheres,[4–8] and uncharged spherical soft particles.[9]

In particular, the reason to study soft particles stems from the desire to explore the behavior of a number of complex fluids composed of nonrigid structures such as polymerically stabilized colloidal spheres,[10] block copolymer micelles,[11] star polymers,[12] hard spheres with a grafted polymer brush,[13] dendritically branched polymers,[14] and others. Additionally, soft particles are particularly important for biological systems because they can be a model for biological cells such as red blood cells and bacteria.[15]

For nondilute systems, the suspension rheology is determined by the interplay between the direct particle-particle interactions and the solvent-mediated hydrodynamic interactions.[16] Their many body nature impose a formidable difficulty for the calculation of rheological quantities such as the shear viscosity of the system. In addition, the fact that many particles are solvent-permeable to some extent complicates the calculation. Thus, for concentrated suspensions, simplifying strategies have been devised to include in an approximate way all these contributions. A very successful approach consists in treating the hydrodynamic interactions by means of a recursive differential procedure in which particles are progressively incorporated to the suspension while the direct excluded-volume interactions *due to crowding effects* are contained in an *effective* volume fraction $\phi_{eff}$. This procedure leads to an universal representation of all experimental results in a master curve for $\eta$ vs. $\phi_{eff}$ indicating that $\phi_{eff}$ is a natural variable for these systems.[17] This differential effective medium technique (DEMT) has been applied to suspensions of hard spheres,[17] emulsions of spherical droplets,[18] suspensions of arbitrarily-shaped hard particles,[19] and suspensions with power-law matrices[20] with excellent results.

a)Electronic mail: cmendoza@iim.unam.mx.

 

The purpose of the present work consists in extending the previous recursive model to incorporate the results for the intrinsic viscosity of soft particles recently obtained utilizing a cell model.[9] We also extend the formalism to treat the case of infinite-frequency viscosity. In this case we have found that $\phi_{eff}$ contains hydrodynamic interactions arising from the so-called relaxation term, in addition to the crowding effects. We compare the resulting expressions with experimental data for the low-shear viscosity of surfactant coated particles and with existing numerical simulations for the high-frequency viscosity of homogeneous porous particles,[16,21] finding an excellent agreement in both cases.

The paper is organized as follows. Section II describes the model and introduces the basic equations for the calculation of $\eta$. In Sec. III we compare the results of our calculation for the low-shear zero-frequency viscosity of concentrated suspensions of soft spheres with other expressions.[15] We test our model with experimental data for sterically stabilized particles in Sec. III A. In Sec. III B we extend our method to the case of the high-frequency viscosity and use our expressions to calculate the infinite-frequency viscosity of porous particles and compare the results with recent numerical simulations.[16,21] Finally, in Sec. IV we present our conclusions.

## II. SYSTEM AND BASIC EQUATIONS

For dilute suspensions, the viscosity $\eta$ can in general be written as

$$\eta(\phi) = \eta_0(1 + [\eta]\phi), \tag{2}$$

where $[\eta]$ is the intrinsic viscosity, which is a single particle property that depends on factors such as shape and porosity. Its calculation is in general difficult, however, recently, Ohshima[9] proposed a theory that allows to calculate $[\eta]$ for suspensions of soft particles. Its cell model is depicted in Fig. 1 where a soft particle is modeled as a spherical hard core of radius $a$ coated with a surface soft layer of thickness $d$. The soft layer may represent a grafted polymer brush[22] as represented in Fig. 1. Thus, the polymer-coated particle has an inner radius $a$ and an outer radius $b = a + d$. The cell model assumes that each soft sphere is surrounded by a virtual shell of outer radius $c$ and the particle volume fraction is then given by

$$\phi = \left(\frac{b}{c}\right)^3. \tag{3}$$

The polymer segments are regarded as resistance centers distributed in the permeable polymer layer, exerting frictional forces $-\gamma\mathbf{u}$ on the liquid flowing in the layer, where $\mathbf{u}$ is the liquid velocity relative to the particle and $\gamma$ is the frictional coefficient. The result of this model is expressed in the following equation:[9]

$$[\eta] = \frac{5}{2}\frac{L_2(\lambda b, a/b)}{L_1(\lambda b, a/b)}, \tag{4}$$

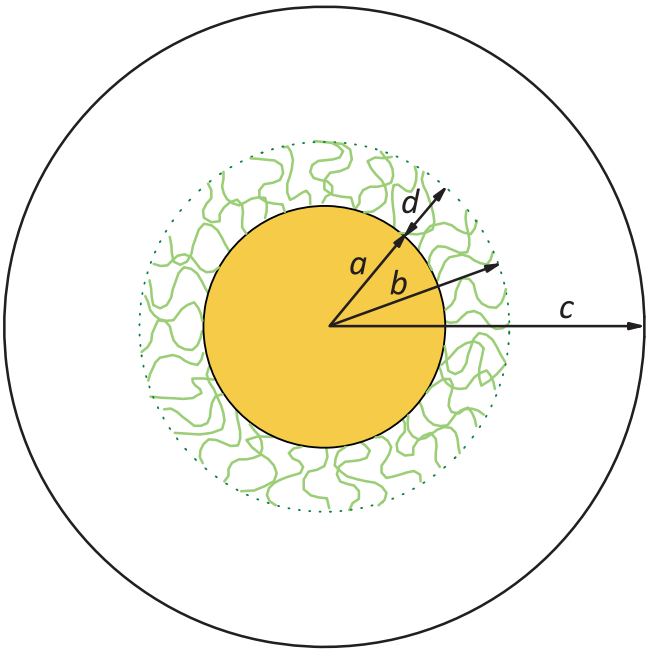


FIG. 1. Schematics of a cell model for a suspension of soft spheres. A hard core of radius $a$ covered by a porous layer of thickness $d$ that may represent a grafted polymer brush. The total radius of the particle is $b = a + d$. The spherical particle is surrounded by a virtual shell of radius $c$ and the volume fraction is $\phi = (b/c)^3$.

where $L_1(\lambda b, a/b)$ and $L_2(\lambda b, a/b)$ are given by

$$\begin{aligned} L_1(\lambda b, a/b) = &-\frac{20(a/b)^2}{(\lambda b)^2} + \left(1 + \frac{2}{3}(a/b)^5 + \frac{30}{(\lambda b)^4}\right. \\ &\left. - \frac{30}{(a/b)(\lambda b)^4} + \frac{10}{(\lambda b)^2} + \frac{10(a/b)^3}{(\lambda b)^2}\right) \\ &\times \cosh(\lambda b - (a/b)\lambda b) \\ &+ \left(1 + 4(a/b)^5 + \frac{30}{(\lambda b)^4} - \frac{30(a/b)}{(\lambda b)^2}\right. \\ &\left. + \frac{10}{(\lambda b)^2} + \frac{10(a/b)^3}{(\lambda b)^2}\right)\frac{\sinh(\lambda b - (a/b)\lambda b)}{(a/b)\lambda b}, \end{aligned} \tag{5}$$

$$\begin{aligned} L_2(\lambda b, a/b) = &\left(1 + \frac{2}{3}(a/b)^5 + \frac{30(a/b)^3}{(\lambda b)^4} - \frac{30(a/b)^2}{(\lambda b)^4}\right. \\ &+ \frac{3}{(\lambda b)^2} - \frac{3}{(a/b)(\lambda b)^2} + \frac{10(a/b)^3}{(\lambda b)^2} \\ &\left. - \frac{12(a/b)^4}{(\lambda b)^2} + \frac{2(a/b)^5}{(\lambda b)^2}\right)\cosh(\lambda b - (a/b)\lambda b) \\ &+ \left(1 - 3(a/b) + 4(a/b)^5 - 2(a/b)^6\right. \\ &+ \frac{30(a/b)^3}{(\lambda b)^4} - \frac{30(a/b)^4}{(\lambda b)^2} \\ &\left. + \frac{3}{(\lambda b)^2} + \frac{10(a/b)^3}{(\lambda b)^2} + \frac{12(a/b)^5}{(\lambda b)^2}\right) \\ &\times \frac{\sinh(\lambda b - (a/b)\lambda b)}{(a/b)\lambda b} \end{aligned} \tag{6}$$

with

$$\lambda = \sqrt{\frac{\gamma}{\eta_0}}. \tag{7}$$

In order to extend the regime of validity of $\eta(\phi)$ to larger concentrations we follow the recursive procedure proposed in Refs. 17–19. In this method, first, we incorporate correlations between particles due to crowding effects in Eq. (2) by writing the viscosity as

$$\eta(\phi) = \eta_0(1 + [\eta]\phi_{eff}), \tag{8}$$

where the effective volume fraction $\phi_{eff}$ is defined by

$$\phi_{eff} = \frac{\phi}{1 - c\phi}, \tag{9}$$

with $c$ a crowding constant. The fact that the particles cannot occupy all the volume of the sample due to geometrical restrictions is taken into account in the crowding factor $c$. For example, for a face centered cubic (FCC) arrangement of identical spheres, the maximum volume that the spheres may occupy is larger than for a random arrangement of spheres, thus, the value of $c$ is different in these two situations. Equation (8) reduces to Eq. (2) at small $\phi$.

Although in this expression $\eta(\phi)$ incorporates the excluded volume corrections, hydrodynamic interactions are ignored and therefore one expects its validity been restricted to low concentrations. To improve it, further corrections must appear due to the hydrodynamic interactions between particles which become increasingly important when increasing the filling fraction. The mentioned correlations can be accounted for by using DEMT techniques.[23] This theoretical method is based on a progressive addition of spheres to the sample in which the new particles interact in an effective way with those added in previous stages.[24] The final result obtained with this procedure is[17–19]

$$\eta(\phi) = \eta_0(1 - \phi_{eff})^{-[\eta]}, \tag{10}$$

or, using the definition of $\phi_{eff}$

$$\eta(\phi) = \eta_0 \left[1 - \left(\frac{\phi}{1 - c\phi}\right)\right]^{-[\eta]}. \tag{11}$$

From this expression it is clear that $c$ depends on the critical volume fraction $\phi_c$ which is the concentration at which the suspension loses its fluidity and is given by

$$c = \frac{1 - \phi_c}{\phi_c}. \tag{12}$$

Thus, the effective volume fraction (9) approaches the bare $\phi$ at low concentrations and becomes 1 at the divergence of the viscosity which occurs at $\phi_c$. Equation (11) together with Eq. (4) are the basic ingredients to calculate the viscosity of soft particles.

If we neglect in our model the excluded volume interactions then $\phi_{eff} = \phi$ and one recovers the Brinkman-Roscoe's result,[25,26] $\eta(\phi) = \eta_0(1 - \phi)^{-[\eta]}$, which contains higher order corrections to the Einstein-like expression, Eq. (2). Since excluded volume interactions have been neglected, then these corrections should be attributed to the hydrodynamic interactions which are implicitly incorporated through the differential procedure.

Note that our model, Eq. (11), *is different from the popular Krieger-Dougherty expression*,[27]

$$\eta(\phi) = \eta_0 \left[1 - \left(\frac{\phi}{\phi_{\max}}\right)\right]^{-[\eta]\phi_{\max}}, \tag{13}$$

where $\phi_{\max}$ is the volume fraction at maximum packing. This expression underestimates the viscosity of the suspension at large volume fractions as explained thoroughly in Ref. 19.

It is important to stress that other differential effective medium theories have been combined previously with effective volume concepts (see, for example, Refs. 28 and 29, and references therein). However, in the case of coated particles, they are usually introduced to take into account the effect of the stabilizer layer and therefore is a single particle property. If the thickness of the stabilizer layer tends to zero then it reduces to the core volume fraction. In contrast, the effective volume fraction introduced in Eq. (9) describes crowding effects which is *a collective effect* and is present even in the case of hard spheres in which the stabilizer layer is absent.

## III. RESULTS AND DISCUSSION

In Fig. 2 we show $\eta(\phi)$ for several values of the parameters $\lambda b$ at $a/b = 0.4$ [panel (a)] and at $a/b = 0.8$ [panel (b)]. It is seen that the viscosity increases with increasing $\lambda b$ and that this effect is more pronounced for smaller values of $a/b$. This means that suspensions of particles with smaller frictional coefficient are less viscous. The limit $\lambda b \to \infty$ corresponds to a very large frictional coefficient and therefore reduces to the hard-sphere case. Panel (c) of Fig. 2 shows $\eta(\phi)$ for several values of the parameters $a/b$ at $\lambda b = 1$ and panel (d) at $\lambda b = 10$. It is seen that the viscosity increases with increasing $a/b$ and that this effect is more pronounced for smaller values of $\lambda b$. This means that particles with thicker soft coronas present less viscosity. The case $a/b = 1$ corresponds to hard-sphere particles since the thickness of the soft corona is zero. The critical volume fraction used in all the curves corresponds to the random close packing of spherical particles $\phi_c = 0.637$.

Recently, Ohshima has extended his cell model to consider concentrated suspensions of spherical soft particles.[15] In this case his expression for the viscosity is

$$\eta(\phi) = \eta_0 \left(1 + \frac{5}{2}\Omega(\lambda b, a/b, \phi)\phi\right), \tag{14}$$

with

$$\Omega(\lambda b, a/b, \phi) = \frac{L_2(\lambda b, a/b, \phi)}{L_1(\lambda b, a/b, \phi)}, \tag{15}$$

where $L_1(\lambda b, a/b, \phi)$ and $L_2(\lambda b, a/b, \phi)$ are somewhat lengthy expressions given in the appendix of Ref. 15. In Fig. 3 we compare our expression with the dilute and concentrated versions of the cell model.[15] It is seen that for low concentrations the cell model gives upper and lower bounds for the viscosity but for increasing volume fractions it underestimates largely the viscosity, particularly for particles with thicker porous layers.

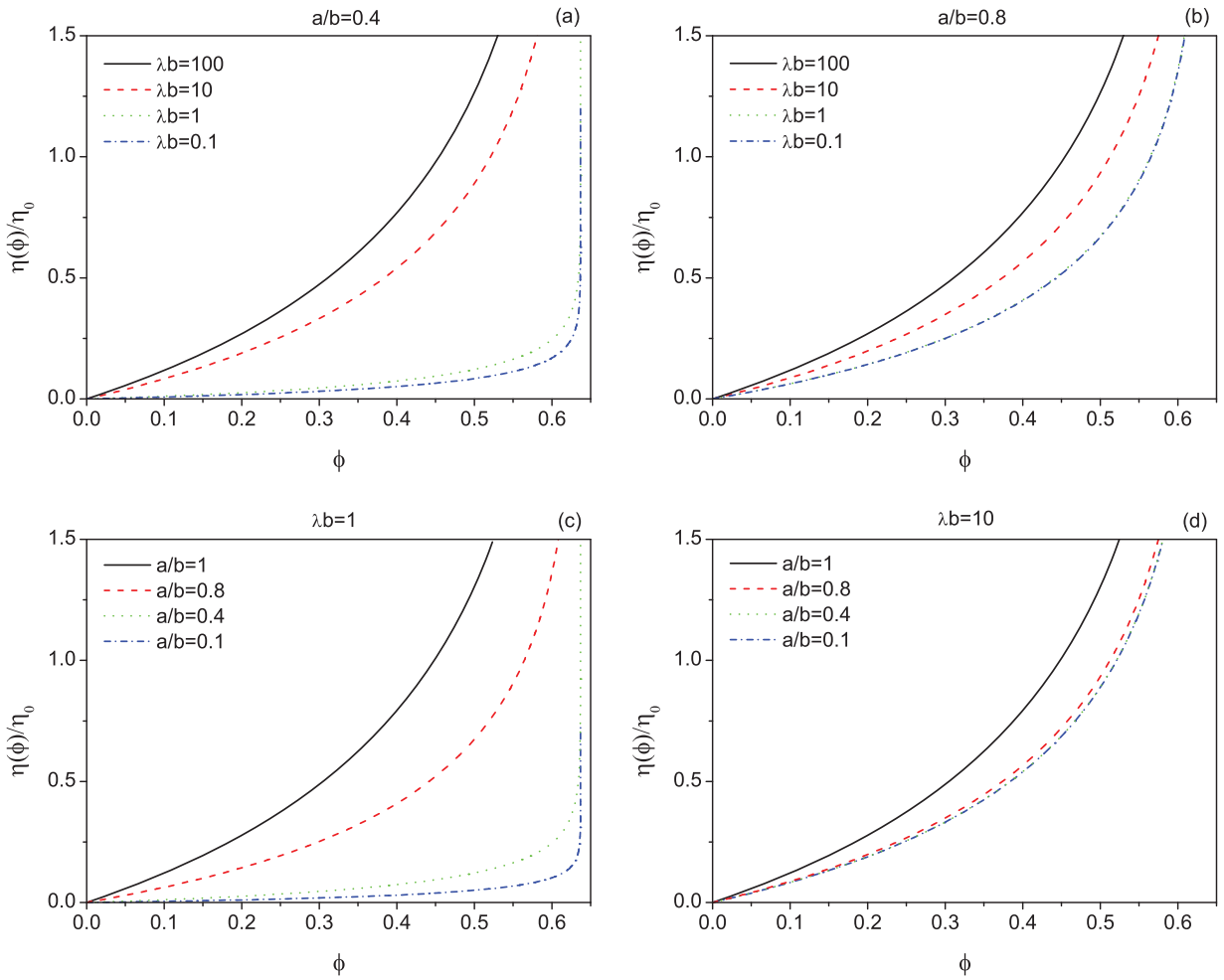


FIG. 2. Relative viscosity $\eta(\phi)/\eta_0$ as function of the particle volume fraction $\phi$ for several values of $\lambda b$ at (a) $a/b = 0.4$ and (b) $a/b = 0.8$; and for several values of $a/b$ at (c) $\lambda b = 1$, and (d) $\lambda b = 10$. In all cases we assumed for the critical volume fraction the random closed packing value for hard spheres, $\phi_c = 0.637$.

### A. Low-shear viscosity of sterically stabilized particles

In this section we apply the DEMT model to the case of sterically stabilized particles. The modification of the viscosity by an adsorbed layer of thickness $d$ (Fig. 1) of a surfactant grafted to a latex particle is studied in Ref. 30. The system studied consists of a poly(styrene) core latex without chemically bound charges (radius: $a = 73$ nm) and a layer of poly(ethylene oxide) chains (length: 80 ethylene oxide units) affixed to the surface of the particles through adsorption of the surfactant Lutensol AT80 (C16-18EO80).

The hydrodynamic thickness of the surfactant layer was determined by small-angle x-ray scattering to be of approximately $d = 12$ nm ($b = a + d = 85$ nm). Since there is no information about the friction coefficient we consider the limits of infinite friction coefficient for which Eq. (4) reduces to $[\eta] = 5/2$, which means that particles are hard spheres of radius $b$, and the limit of zero friction coefficient for which Eq. (4) reduces to $[\eta] = 5/2(a/b)^3$, which corresponds to a hard core surrounded by a perfectly porous shell or radius $b$.

In Fig. 4 we plot the zero-shear viscosity as given by our model in these two limits as a function of the volume fraction of the *coated* particle, $\phi = (b/c)^3$. We took $\phi_c = 0.58$ which corresponds to the glass transition for this system. As can be seen, the hard sphere limit fits very well the experimental data while the soft limit lies far below. Thus, our model confirms the well known fact that surfactant-coated particles behave as hard spheres. Note that the data are very well described by our model which predicts the correct divergence in the viscosity at the glass transition in contrast to the well known Krieger-Dougherty expression,[27] Eq. (13), which does not fit the data very well and predicts a value $\phi_c = 0.53$, which is too low.[30]

In the derivation of Eq. (4) it is assumed that the polymer layer of thickness $d$ has uniform density. Although this is a reasonable approximation for a polymer layer adsorbed on a colloidal particle, it is not the case for a polymer brush (see, for example, Ref. 31 and references therein). Specifically, the amount of solvent and its flow through the porous layer will be different for a uniform and a nonuniform density profiles.[32,33] A more accurate description would consider a distribution of the resistance centers in the permeable polymer layer dependent on the density profile of the polymer brush. This could be incorporated into the model by using, for example, a position-dependent frictional coefficient $\lambda$. However, such refinement

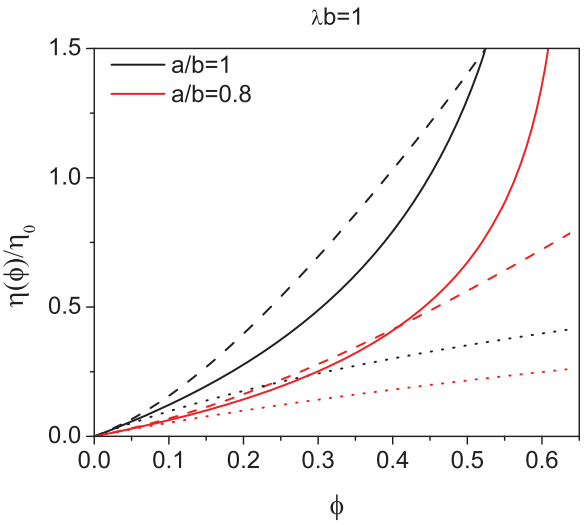


FIG. 3. Reduced viscosity $\eta(\phi)/\eta_0$ as function of the volume fraction $\phi$ at $\lambda b = 1$ for $a/b = 1$ (black lines) and $a/b = 0.8$ (red lines). The present model lies between the dilute and concentrated cell model results at low $\phi$ but increases more rapidly for large $\phi$ particularly for smaller values of $a/b$ (thicker porous layers).

does not seem to be needed since one can always absorb its effects considering a uniform layer with an average value for $\lambda$. A more important effect would arise in systems of polymer-coated particles in which the length of the polymer layer is of the order of the core diameter. In this case, the suspension may present a large relative interparticle penetration, especially at large concentrations.[34] Under certain conditions the result of these interactions appears as a shoulder in the viscosity-concentration curves.[35,36] Thus, a direct application of our model would not fit the experimental data accurately at this second regime where interparticle penetration is important.

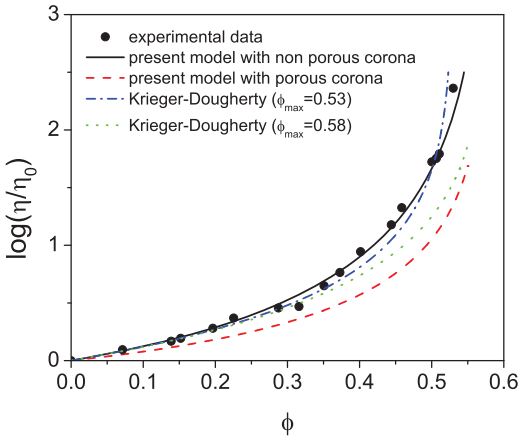


FIG. 4. Relative static low-shear viscosity $\eta/\eta_0$ as function of the volume fraction $\phi = (b/c)^3$ for the latex covered by the surfactant Lutensol AT80. The symbols are the experimental data of Ref. 30. The solid line displays the result of our model for suspensions of hard spheres. The dashed line shows our model considering a frictionless soft corona. In both fits $\phi_c = 0.58$, corresponding to the glass transition for this system. The dotted and dashed-dotted lines correspond to the Krieger-Dougherty model for hard spheres with $\phi_{\max} = 0.58$ and $\phi_{\max} = 0.53$, respectively.

### B. High-frequency viscosity of porous-particle suspensions

In this section we probe the accuracy of our model with recent simulation results[16,21] for the low-shear high-frequency viscosity, $\eta_\infty$, of a monodisperse suspension of nonoverlapping porous spherical particles as a function of volume fraction and porosity.

The high-frequency viscosity, $\eta_\infty$, is related to the static viscosity by means of the relation $\eta = \eta_\infty + \Delta\eta$. Here, the so-called relaxation term $\Delta\eta > 0$ is an additional contribution arising from the time integrated relaxation of the shear-distorted particles microstructure and depends on both, the direct and hydrodynamic interactions.[21] Thus, at low volume fractions one can write

$$\eta_\infty/\eta_0 \simeq 1 + [\eta]\phi_{eff} - \Delta\eta/\eta_0, \tag{16}$$

where we have used Eq. (8) to include crowding effects. Since the relaxation term arises from the interactions between particles, then, the leading-order term in an expansion in powers of $\phi$ should be quadratic.[37,38] Therefore, to leading order in $\phi$,

$$\Delta\eta/\eta_0 \simeq [\eta]\alpha\phi^2, \tag{17}$$

with $\alpha$ a porosity-dependent positive coefficient. Substituting Eqs. (9) and (17) in Eq. (16) we find

$$\eta_\infty/\eta_0 \simeq 1 + [\eta]\phi + [\eta](c-\alpha)\phi^2, \tag{18}$$

where we have kept up to second-order terms in $\phi$. The last equation can be approximated by

$$\eta_\infty/\eta_0 \simeq 1 + [\eta]\frac{\phi}{1-(c-\alpha)\phi}. \tag{19}$$

This equation can now be used as starting point of the DEMT procedure exactly as before if we define a new effective volume fraction

$$\phi_{eff}^\infty = \frac{\phi}{1-c_\infty\phi}, \tag{20}$$

where

$$c_\infty = c - \alpha. \tag{21}$$

The resulting expression for $\eta_\infty/\eta_0$ is

$$\eta_\infty(\phi) = \eta_0(1-\phi_{eff}^\infty)^{-[\eta]}, \tag{22}$$

or, using Eq. (20)

$$\eta_\infty(\phi) = \eta_0\left(1-\frac{\phi}{1-c_\infty\phi}\right)^{-[\eta]}. \tag{23}$$

Equation (22) is identical to Eq. (10) but with $\phi_{eff}^\infty$ replacing $\phi_{eff}$. It is important to remark that $c_\infty$ contains hydrodynamic contributions in addition to the direct excluded volume interactions and since $\alpha$ is positive then $c_\infty$ does not necessarily has to be positive in contrast to $c$ which is always positive.

In the simulations,[16,21] each particle is modeled as a rigid sphere of radius $b$ and constant Darcy porosity $k$, with the fluid flow inside the particle described by the Debye-Bueche-Brinkman equation.[4,5] The many-body hydrodynamic interactions are fully accounted for by using a precise hydrodynamic multipole method. The results of these simulations for porosity values that span the range from nonporous to highly

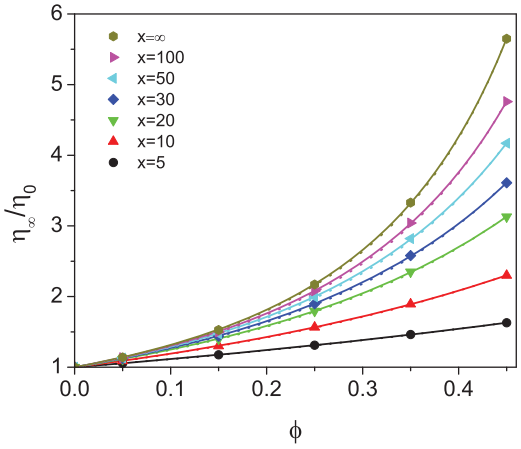


FIG. 5. Low-shear high-frequency viscosity, $\eta_\infty/\eta_0$, of uniformly porous spheres for porosities as indicated ($x = \infty$ corresponds to nonporous hard-spheres). Simulation results (symbols), the present model in the porous sphere limit, with $x$ given by the simulations and $c_\infty$ the only fitting parameter, Eqs. (23) and (24) (dotted lines), and with $x$ as an additional fitting parameter (solid lines).

porous particles are shown by the symbols in Fig. 5. The inverse porosity is given by $x \equiv \kappa b$, where $\kappa^{-1} = \sqrt{k}$ is the hydrodynamic penetration depth.[16] In the zero-penetration limit $x \to \infty$, hard-spheres with stick boundary conditions at the surface are recovered.

Taking the limit $a \to 0$ in Eqs. (5) and (6), the intrinsic viscosity Eq. (4) reduces to the homogeneous porous particle limit[4,5]

$$[\eta] = \frac{5}{2}\Omega_v(x) = \frac{5}{2}\frac{G(x)}{1+\frac{10G(x)}{x^2}}, \tag{24}$$

where

$$G(x) = 1 + \frac{3}{x^2} - \frac{3\coth(x)}{x}, \tag{25}$$

and we have made the identification[21] $x \equiv \lambda b$. These expressions agree with the results of Natraj and Chen[39] for the effective viscosity of a dilute suspension of uncharged porous spheres of radius $b$. Tabulated values of $[\eta]$ calculated using Eq. (24) are shown in Table I. Equation (23) combined with Eq. (24) gives the prediction of our model for the high-frequency viscosity of homogeneous porous spheres. Substituting the values of $x$ corresponding to the simulations we obtain the dotted curves shown in Fig. 5. Here, we used $c_\infty$ as the only fitting parameter and it is shown in Table II. The fact that $c_\infty$ is negative implies that the high-frequency viscosity in the regime described by our model does not diverge, as it is clearly shown in the simulations. The viscosity as function of the inverse porosity $x$ for three different values of $\phi$ is shown

TABLE I. Intrinsic viscosity, $[\eta]$, as calculated from Eq. (24) and Huggins coefficient, $k_H$, as obtained from the numerical simulation of Ref. 16.

| $x$ | 5 | 10 | 20 | 30 | 50 | 100 | ∞ |
|---|---|---|---|---|---|---|---|
| $[\eta]$ | 1.076 | 1.701 | 2.099 | 2.236 | 2.344 | 2.423 | 2.500 |
| $k_H$ | 0.5321 | 0.6270 | 0.7019 | 0.7323 | 0.7587 | 0.7796 | 0.8004 |

TABLE II. Intrinsic viscosity, $[\eta]$, as calculated from Eq. (24) and Huggins coefficient, $k_H$, as obtained from our model, Eq. (27), with $c_\infty$ as the only fitting parameter. The quadratic order coefficient, $[\eta]\alpha$, of the relaxation term is calculated from Eqs. (11), (16), and (23) assuming $c = 0.5698$ ($\phi_c = 0.637$).

| $x$ | 5 | 10 | 20 | 30 | 50 | 100 | ∞ |
|---|---|---|---|---|---|---|---|
| $[\eta]$ | 1.076 | 1.701 | 2.099 | 2.236 | 2.344 | 2.423 | 2.500 |
| $c_\infty$ | −0.5161 | −0.3555 | −0.1572 | −0.0628 | 0.0336 | 0.1182 | 0.2226 |
| $[\eta]\alpha$ | 1.1686 | 1.5739 | 1.5259 | 1.4146 | 1.2571 | 1.0946 | 0.8681 |
| $k_H$ | 0.4850 | 0.5850 | 0.6633 | 0.6956 | 0.7276 | 0.7551 | 0.7890 |

in Fig. 6. It can be seen that the agreement between theory and simulation is excellent.

Although we have presented results only for the high-frequency viscosity for the given system of rigid porous particles, the static low- and high-shear viscosity for the same system can also be computed using Eq. (11). The values that the fitting parameter $c$ adopts in each case are presumably the same as for the case of hard spheres. It has been shown[17] that the static viscosity of hard spheres at low-shear stress is well described using $c = 0.5698$ or equivalently, $\phi_c = 0.637$, which is the random close packing of spheres while for high-shear stress, $c = 0.3504$ or $\phi_c = 0.7405$ which corresponds to the FCC close packing fraction. This difference in $\phi_c$ is attributed to the fact that in the latter situation the particles are ordered as a result of the large shear flow. Using these fitting parameters, the predictions of our model, Eq. (11) with (24) could be tested with computer simulations when they become available. Here we only show the relaxation term $\Delta\eta = \eta - \eta_\infty$ as extracted from Eqs. (11) and (23) assuming a random distribution of spheres $c = 0.5698$ ($\phi_c = 0.637$) and the values of $c_\infty$ given in Table II. The results are shown with thick lines in Fig. 7. The coefficient of the quadratic order of the relaxation term, Eq. (17), can be extracted from Eqs. (12) and (21). This is shown in Table II where again we have assumed $\phi_c = 0.637$. The corresponding relaxation term to quadratic order is shown with thin lines in Fig. 7.

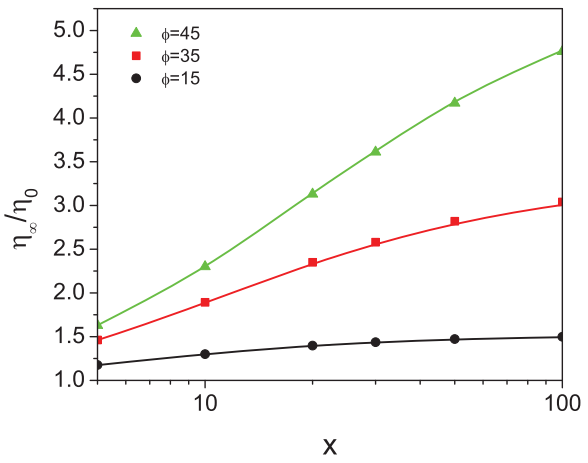


FIG. 6. Low-shear high-frequency viscosity, $\eta_\infty/\eta_0$, as function of the porosity for uniformly porous spheres. Simulation results (symbols). The present model in the porous sphere limit (curves).

At small volume fractions the viscosity $\eta_\infty$ can be expanded in a virial series as

$$\eta_\infty(\phi) = \eta_0(1 + [\eta]\phi + k_H[\eta]^2\phi^2 + ...). \tag{26}$$

In contrast to $[\eta]$ that is a single-particle property, the Huggins coefficient, $k_H(x)$ accounts for two-body hydrodynamic interactions. Using their numerical simulation data, in Ref. 16 this coefficient is calculated to high-precision for porous spheres at several values of $x$ and the results are tabulated in Table I. On the other hand, the present model, given by Eq. (23), in the porous sphere limit [Eq. (24)] gives the following expression for $k_H(x)$:

$$k_H(x) = \frac{40 + 5(x^2 - 4)/(1 + c_\infty) + 2x^4[2 - 1/(1 + c_\infty)]/[3 + x^2 - 3x\coth(x)]}{10x^2/(1 + c_\infty)}. \tag{27}$$

Tabulated values of $k_H$, Eq. (27), for this model are also shown in Table II, where the values of $c_\infty$ used to calculate $k_H$ are the ones that best fitted the simulation data shown in Fig. 5.

It is interesting to ask if our model can give reliable predictions about the inverse viscosity parameter $x$ if this information is not provided and only the data points are given. This means that in our model $x$ is a second fitting parameter. The fitted values of $x$ are shown in Table III together with the value of $k_H$ obtained using Eq. (27) as before. Notice that this two-fitting variable procedure gives a slightly better agreement with the experimental data points as shown by the solid lines in Fig. 5.

Based on the results of their numerical simulations together with a virial expansion up to third order in $\phi$ the authors of Ref. 16 propose an approximate analytic expression for $\eta_\infty$ in the form of a generalized Saito formula

$$\frac{\eta_\infty}{\eta_0} = 1 + [\eta]\phi\frac{1 + S}{1 - \frac{2}{5}[\eta]\phi(1 + S)}, \tag{28}$$

where the Saito function is approximated by a third-order in $\phi$ polynomial

$$S(x, \phi) = b_1(x)\phi + b_2(x)\phi^2 + b_3(x)\phi^3, \tag{29}$$

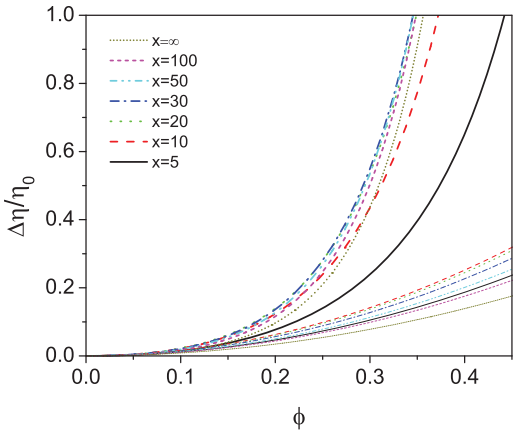


FIG. 7. Relaxation term $\Delta\eta/\eta_0$ as function of the volume fraction $\phi$ at different values of $x$. Thin lines correspond to the quadratic approximation, Eq. (17), while thick lines are obtained from Eqs. (11), (16), and (23) using $\phi_c = 0.637$.

with

$$b_1(x) = \left(k_H - \frac{2}{5}\right)[\eta], \tag{30}$$

which is calculated using the values of $[\eta]$ obtained from Eq. (24) and from the numerical simulation for $k_H$. Then, the coefficients $b_2(x)$ and $b_3(x)$ are obtained *from a best fit* of the simulation data for $\eta_\infty$ in the range $\phi \leq 0.45$ (see Ref. 16). The curves for the viscosity obtained from this expression (28) are indistinguishable of the solid lines of Fig. 5 corresponding to our model with two fitting parameters. Notice that the curves obtained with the one fitting parameter version of our model are almost identical with the ones obtained using two parameters. Thus, the use of only one parameter seems to be accurate enough for any practical purpose and we think it is preferable over the generalized Saito expression (28) since this last formula has more fitting coefficients and is not supported by a theoretical derivation.

A very appealing feature of Eq. (23) is that it allows to plot $\eta$ in a universal curve independent of $c_\infty$ and $x$ (or independent of $c_\infty$, $\lambda b$ and $a/b$ in the most general case) if we express it as function of $\phi_{eff}^\infty$ instead of $\phi$. This is done in Fig. 8 where $\phi_{eff}^\infty$ is calculated using Eq. (20) and the values of $c_\infty$ given in Table II. Additionally, we have plotted the experimental results for the viscosity of the sterically stabilized particles of Sec. III A. In all cases the data collapses perfectly into the master curve.

Alternative simple routes to calculate the high-frequency viscosity of porous particles have been proposed. One of these simplifying strategies known as effective radius model

TABLE III. Fitted viscosity $x$, intrinsic viscosity, $[\eta]$, as calculated from Eq. (24) and Huggins coefficient, $k_H$, as obtained from our model, Eq. (27), with $c_\infty$ and $x$ as fitting parameters. The quadratic order coefficient, $[\eta]\alpha$, of the relaxation term is calculated from Eqs. (11), (16), and (23) assuming $c = 0.5698$ ($\phi_c = 0.637$).

| $x$ | 5 | 10 | 20 | 30 | 50 | 100 | $\infty$ |
|---|---|---|---|---|---|---|---|
| $x$ (fit) | 5.07 | 10.5 | 23.8 | 41.6 | 100 | 2604 | $\infty$ |
| $[\eta]$ | 1.090 | 1.739 | 2.164 | 2.311 | 2.423 | 2.497 | 2.500 |
| $c_\infty$ | −0.5482 | −0.4044 | −0.2172 | −0.1236 | −0.0230 | 0.0704 | 0.2226 |
| $[\eta]\alpha$ | 1.2031 | 1.6571 | 1.6519 | 1.5505 | 1.3898 | 1.2104 | 0.8681 |
| $k_H$ | 0.4558 | 0.5550 | 0.6307 | 0.6628 | 0.6968 | 0.7284 | 0.7890 |

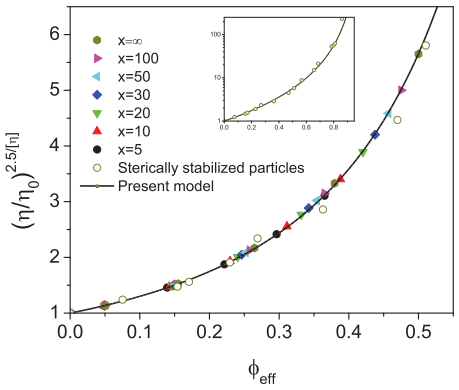


FIG. 8. Master curve for the viscosity. $\eta$ represents the zero-shear high-frequency viscosity $\eta_\infty$ for the case of the homogeneous porous particles of Ref. 16 and represents the zero-shear static viscosity for the sterically stabilized particles of Ref. 30. In the inset we show the master curve for the latter case in the whole experimental range of volume fractions. $\phi_{eff}$ represents $\phi_{eff}^{\infty}$ in the high-frequency case.

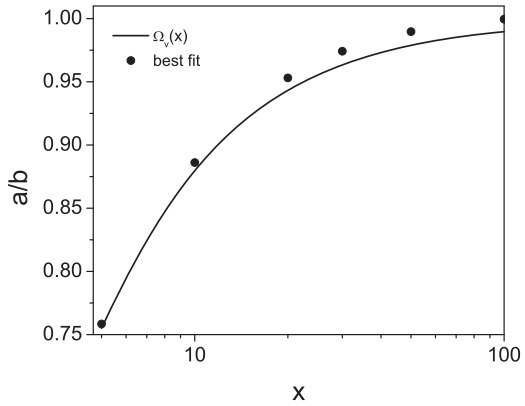


FIG. 9. Ratio of the soft to core radii $a/b$, for the hydrodynamic radius model as calculated using Eq. (32) (curve) and as obtained from our model in the two fitting parameter case (dots).

consists in introducing a porosity-dependent effective hard-sphere of radius $a$ and to map the shear viscosity of porous spheres to that of nonporous ones with a smaller radius and a smaller volume fraction.[40] This strategy however, has no sound theoretical basis and in general does not lead to satisfactory results.[16] The reason for this is that two effective nonporous particles are allowed to approach each other up to the center to center distance $2a < 2b$. However, the rigid skeleton of the actual porous particles of radius $b$ does not allow them to overlap, and the statistical distribution function of the effective particles should take this into account. A more refined model,[16] referred to as hydrodynamic radius model takes this fact into account by considering that the porous sphere of radius $b$ is described as a soft particle with a hard core of porosity-dependent effective radius $a$, and an outer excluded volume of radius $b$, which enters into the statistical distribution through the nonoverlap requirement. This model gives more accurate results as compared to the effective radius model but the viscosity must be computed numerically.

A similar approach can be done using the model proposed in the present work. Indeed, if we consider that the outer core of the soft sphere do not exert frictional forces on the liquid flowing through it, that is, $\lambda = 0$, then Eqs. (5) and (6), simplify considerably and one gets

$$[\eta] = \frac{5}{2}\left(\frac{a}{b}\right)^3. \tag{31}$$

If we define the porosity dependent effective radius $a$ by

$$\left(\frac{a}{b}\right)^3 = \Omega_v(x), \tag{32}$$

then one recovers Eq. (24). In other words, in our model, the shear viscosity of a porous homogeneous particle of radius $b$ and inverse porosity $x$ is *identical* to that of a soft particle with a hard core of porosity-dependent radius $a$ given by Eq. (32) with a nonfrictional outer core or radius $b$. Thus, in our approach, the hydrodynamic radius model is an *exact* representation of a homogeneously porous particle. In Fig. 9 we show with solid lines the result for $a/b$ as obtained from Eq. (32) and the dots represent the values obtained when $x$ given in Table III are substituted in Eq. (32).

## IV. CONCLUSIONS

In this paper we have presented a simple model for the calculation of the static and high-frequency viscosities as function of particle concentration for suspensions of soft spherical particles consisting of a hard core of radius $a$ covered with a porous layer of thickness $d = b - a$.

The model considers excluded volume correlations between the particles through an effective filling fraction $\phi_{eff}$, whereas the hydrodynamic interactions between particles are taken into account through a differential effective-medium approach.[17–19] Additionally, a cell model[15] is used to calculate the intrinsic viscosity $[\eta]$ of the soft particles as function of the friction parameter $\lambda b$ and the ratio $a/b$. The limit $\lambda b \to \infty$ or $a/b \to 1$ corresponds to the intrinsic viscosity of hard spheres while the limit $a \to 0$ reduces to the intrinsic viscosity of a homogenous porous particle of porosity $x = \lambda b$. Our results are summarized by Eqs. (4) and (11). Although the model contains three parameters, $\lambda b$, $a/b$, and $\phi_c$, in principle $\lambda b$ and $a/b$ could be determined experimentally leaving $\phi_c$ as the only fitting parameter.

We have applied our model to the case of the zero-frequency low-shear viscosity of sterically stabilized particles[30] and found that a hard-sphere limit is enough to describe the data accurately with a $\phi_c = 0.58$, corresponding to the glass transition volume fraction. This result improves the one obtained with the Krieger and Dougherty expression which underestimates largely the value of $\phi_c$.

In the case of the high-frequency viscosity we have shown that $\phi_{eff}$ contains hydrodynamic interactions arising from the relaxation term in addition to the crowding effects. We have also tested the accuracy of our model with recently obtained numerical data for the high-frequency viscosity of homogeneous porous particles[16,21] with excellent results. Additionally, we have found that the homogenous porous particle limit of our model is completely *equivalent* to a hydrodynamic radius model in which the homogeneous

porous particle is replaced by a core-shell particle with $a/b$ given by Eq. (32). Let us stress that the form of the expression for the viscosity as function of $\phi_{eff}$ given by our model, Eq. (10), leads to an universal representation that may be used to reduce both experimental and theoretical results to a master curve[17–19] which is independent of the experimental details or the softness of the particles.

Although in the present paper we have considered a suspension of uncharged soft particles, the case of charged soft spheres suspended in an electrolyte can also be treated with the proposed method by replacing the intrinsic viscosity, Eq. (4), by

$$[\eta] = \frac{5}{2}(1+p)\frac{L_2(\lambda b, a/b)}{L_1(\lambda b, a/b)}, \tag{33}$$

where $p$ is the primary electroviscous coefficient.[15] Our method can also be used to calculate other transport properties like the diffusion coefficients. Work along this line is currently under progress. As a final remark, let us mention that a direct application of the present model to systems of particles coated by a thick polymer layer would only give approximate results since interactions between the outer segments of the polymers that belong to different particles are being ignored. However, such interactions can also be modeled and will be the subject of a future work.

## ACKNOWLEDGMENTS

I appreciate the hospitality of Prof. Andrea J. Liu and the Department of Physics and Astronomy of the University of Pennsylvania where this work was carried out during a sabbatical leave. I would like to thank Iván Santamaría-Holek for illuminating discussions and useful comments. I acknowledge support provided by DGAPA-UNAM through a Sabbatical Fellowship and by grants UPENN-MRSEC DMR05-20020 and DGAPA IN-115010.

[1] A. Einstein, Ann. Phys. **19**, 289 (1906); **34**, 591 (1911).
[2] G. B. Jeffery, Proc. R. Soc. London, Ser. A **102**, 715 (1922).
[3] G. I. Taylor, Proc. R. Soc. London, Ser. A **138**, 41 (1932).
[4] H. C. Brinkman, Proc. R. Dutch Acad. Sci. **50**, 618 (1947).
[5] P. Debye and A. M. Bueche, J. Chem. Phys. **16**, 573 (1948).
[6] Q. Yu and P. N. Kaloni, J. Appl. Math. Phys. **39**, 937 (1988).
[7] T. Baczynska and J. Glowinsky, Rheol. Acta **36**, 483 (1997).
[8] H. Ohshima, Colloids Surf., A **347**, 33 (2009).
[9] H. Ohshima, Langmuir **24**, 6453 (2008).
[10] D. Vlassopoulos, G. Fytas, S. Pispas, and N. Hadjichristidis, Physica B **296**, 184 (2001).
[11] A. P. Gast and W. B. Russel, Phys. Today **51**, 24 (1998).
[12] A. N. Semenov, D. Vlassopoulos, G. Fytas, G. Vlachos, G. Fleischer, and J. Roovers, Langmuir **15**, 358 (1999).
[13] J.-C. Castaing, C. Allain, P. Auroy, and A. Pouchelon, Europhys. Lett. **36** 153 (1996).
[14] A. Asteriadi, R. Sigel, D. Vlassopoulos, G. Meier, J. R. Dorgan, and D. M. Knauss, Macromolecules **37**, 1016 (2004).
[15] H. Ohshima, Langmuir **26**, 6287 (2010).
[16] G. C. Abade, B. Cichocki, M. L. Ekiel-Jezewska, G. Nägele, and E. Wajnryb, J. Chem. Phys. **133**, 084906 (2010).
[17] C. I. Mendoza and I. Santamaría-Holek, J. Chem. Phys. **130**, 044904 (2009).
[18] C. I. Mendoza and I. Santamaría-Holek, Appl. Rheol. **20**, 23493 (2010).
[19] I. Santamaría-Holek and C. I. Mendoza, J. Colloid Interface Sci. **346**, 118 (2010).
[20] R. I. Tanner, F. Qi, and K. D. Housiadas, J. Non-Newtonian Fluid Mech. **165**, 1677 (2010).
[21] G. C. Abade, B. Cichocki, M. L. Ekiel-Jezewska, G. Nägele, and E. Wajnryb, J. Phys.: Condens. Matter **22**, 322101 (2010).
[22] J. M. Brader, J. Phys.: Condens. Matter **22**, 363101 (2010).
[23] J. W. Bullard, A. T. Pauli, E. J. Garboczi, and N. S. Martys, J. Colloid Interface Sci. **330**, 186 (2009).
[24] T. G. M. van de Ven, *Colloidal Hydrodynamics* (Academic Press, London, 1989).
[25] H. C. Brinkman, J. Chem. Phys. **20**, 571 (1952).
[26] R. Roscoe, Br. J. Appl. Phys. **3**, 267 (1952).
[27] I. M. Krieger and T. J. Dougherty, Trans. Soc. Rheol. **3**, 137 (1959).
[28] J. Mewis and J. Vermant, Prog. Org. Coat. **40**, 111 (2000).
[29] D. Quemada, Eur. Phys. J.: Appl. Phys. **1**, 119 (1998).
[30] A. Weiss, N. Dingenouts, M. Ballauff, H. Senff, and W. Richtering, Langmuir **14**, 5083 (1998).
[31] F. Lo Verso, S. A. Egorov, A. Milchev, and K. Binder, J. Chem. Phys. **133**, 184901 (2010).
[32] S. T. Milner, Macromolecules **24**, 3704 (1991).
[33] G. S. Grest, Adv. Polym. Sci. **138**, 149 (1999).
[34] P. A. Nommensen, D. van den Ende, M. H. G. Duits, and J. Mellema, Langmuir **17**, 5757 (2001).
[35] J. Roovers, Macromolecules **27**, 5359 (1994).
[36] B. Loppinet, G. Fytas, D. Vlassopoulos, C. N. Likos, G. Meier, and G. J. Liu, Macromol. Chem. Phys. **206**, 163 (2005).
[37] B. Cichocki and B. U. Felderhof, Phys. Rev. A **43**, 5405 (1991).
[38] A. J. Banchio, G. Nägele, and J. Bergenholtz, J. Chem. Phys. **111**, 8721 (1999).
[39] V. Natraj and S. B. Chen, J. Colloid Interface Sci. **251**, 200 (2002).
[40] T. Eckert and W. Richtering, J. Chem. Phys. **129**, 124902 (2008).